Fatigue analysis of FDM materials

John Lee and Adam Huang
Mechanical Engineering, University of Arkansas, Fayetteville, Arkansas, USA

Abstract

Purpose – The purpose of this paper is to determine the effects of fatigue on fused deposition modeling rapid prototyped acrylonitrile butadiene styrene (ABS) materials.

Design/methodology/approach – FDM dog bones based on UNI EN ISO 527-1 (1997) were tested at 100, 80, 60, and 40 per cent nominal values of the ultimate stress for nine different print orientations. The samples were cyclically stressed in a tensile tester at 25.4 mm/min (extension) and relaxed at 12.7 mm/min.

Findings – Although FDM ABS has a tensile strength that is relatively close to that of the bulk material, up to 80 percent, its ability to absorb energy before fracture has a tremendous amount of room for improvement. FDM ABSplus (P430) material properties are noticeably more isotropic than the predecessor, ABS (P400). The ABSplus fractures in the order of thousands of cycles at 40 percent of ultimate stress load, while the ABS exhibits the similar cycle limits at 60 percent of its ultimate stress load.

Practical implications – FDM ABS parts are limited in fatigue characteristics even though they exhibit similar ultimate stress limits as with bulk materials, warranting further research in improving FDM parts expected to experience cyclical loads.

Originality/value – This paper adds knowledge to the limited fatigue data in literature for FDM ABS. It investigated the load cyclic data of fused deposition modeled ABS through analyzing its cycle-by-cycle strain energy, providing another means of identifying the fatigue characteristics of materials.

Keywords Fatigue, FDM, Rapid prototypes

Paper type Research paper

Introduction

Rapid prototyping (RP) of polymer-based materials is now a well-known technology for obtaining a quick and relatively accurate model for design checks and visual representations. In recent years, such rapid prototyped parts from high-strength polymers and polymer composites have seen limited, or conspired for, use in replacing load-bearing parts, often as a cost-effective alternative to limited production runs or designs of complex geometries. When first introduced in the mid-1980s, in the form of stereolithography (Hull, 1986), rapid prototyped parts yielded significantly inferior mechanical properties when compared to other manufacturing methods of the same materials. However, advancements through two decades of experiences have resulted in materials of increasing strength while maintaining its core capability of shaping complex structures, often not possible through conventional manufacturing techniques, leading to new and novel applications such as in the bio-medical field (Ciocca and Fantini, 2009; Owida and Chen, 2011) and aerospace applications (Danehy and Alderfer, 2008; Kroll and Dror, 2011). Inspired by these recent developments, the research described here sought to characterize and understand the fatigue characteristics of parts fabricated by the layered methods of fused deposition modeling (FDM). As an archetype of the commonly used, low-cost, structural RP part, the acrylonitrile butadiene styrene (ABS) FDM by Stratasys® is used for this study.

In general, RP technologies typically do not lend itself directly to engineering application. Even though the bulk properties of materials used by various RP technologies have been well-known in the literature, most rapid prototyped parts exhibit anisotropic and/or modified material properties from its bulk. For example, the mechanical properties of a common structural plastic, ABS, e.g. plastic used for LEGO™, is well-known but its bulk properties cannot be used to design parts fabricated through FDM. This is due to the anisotropy of the FDM's continuously layered fabrication process which reduces its mechanical strength. Using the Stratasys® P400 *ABS* material, Ahn and Montero (2002) have shown that injection molded parts exhibited an ultimate stress of 26 MPa (~3.77 ksi) as compared against the reported value of 22 MPa (~3.19 ksi) using FDM (Fortus, 2007) for the best print orientation. There are methods of rapid prototyped polymeric parts other than FDM that do yield near or complete isotropy of material strength. Unfortunately they often experience a decay of material property over time; such as those made from photo-structured resins due to continued UV-photon exposures in most operational environments.

In general, the static mechanical properties of RP materials can be found in the literature (Ahn and Montero, 2002) or through the manufacturer's specification

The current issue and full text archive of this journal is available at **www.emeraldinsight.com/1355-2546.htm**

Rapid Prototyping Journal
19/4 (2013) 291–299

[DOI 10.1108/13552541311323290]

The authors would like to thank the University of Arkansas allowing the use of the Tensile Test equipment and facilities. They would also like to thank the Arkansas Space Grant Consortium for their assistance in the materials testing.

Received: 9 November 2011
Revised: 8 March 2012
Accepted: 8 March 2012

Rapid Prototyping Journal
Volume 19 · Number 4 · 2013 · 291–299

sheets (Fortus, 2007, 2011). However, this cannot be said for information relating to RP materials subjected to cyclical loads and their fatigue characteristics; the knowledge of which are critical in most load bearing applications. The work presented here focuses on characterizing the fatigue properties of two generations of the baseline FDM RP materials (*ABS* and *ABSplus*) through subjecting flat dog-bones to cyclical loads. A tensile tester is used to provide the high resolution stress-displacement data to simulate every single load cycle to gain understanding of fatigue characteristics in addition to generating design rules for designing parts expected to experience repeated stresses. Thus, only one material sample of each type of each orientation is tested here for cyclical loads due to its time laborious procedure. Nevertheless, the methodology presented here provides the "first-look" data to gain greater understanding of FDM ABS fatigue characteristics and serves as a model for future testing of RP fabricated materials.

Experimental setup

FDM, which has been around commercially since the early 1990s, creates three dimensional objects by discharging a thermoplastic onto a base member at a controlled rate (Crump, 1992). A Stratasys® Dimension, introduced in 2002, was used to print the *ABS* (P400) test specimens which were printed with the "breakaway" support material (P400-RP). The newer *ABSplus* (P430) material was printed using the Dimension Elite, along with a newer soluble material (P400-SR). The printer is enclosed in a temperature controlled chamber and builds the rapid prototyped model in layers using a dual nozzle print head. In sequential order, one print head extrudes the model material, while the other print head extrudes a support material. In the experiments reported here, the solid model file created using SolidWorks is loaded into the Stratasys® software package, CatalystEX™, which generates the print path. The print path prescribes where to extrude model material and where support material is necessary to maintain the shape of the model. The dual head allows for the model to be built in stacked layers of model material and support material, when necessary, without any tool changeover.

The geometry of each rapid prototyped dog-bone specimen followed the UNI EN ISO 527-1 (1997) standard which specifies a 10 mm by 4 mm cross-section with a gauge length of 80 mm. However, the printed cross-sectional area varied, but was generally closer to 4.25 mm by 10.16 mm for ABS and 4.05 mm by 10.1 mm for *ABSplus*. The properties of material as set by Catalyst were 0.254 mm (0.01 in) resolution and solid for *ABS* and 0.178 mm (0.007 in) resolution and solid for *ABSplus*. For rapid prototyped parts, it is common knowledge that the print orientation and pattern affects the material properties (Ahn and Montero, 2002). The test specimens tested here used the default model pattern generated by CatalystEX™. To adequately quantify the material properties of the rapid prototyped material, it was necessary to test in a variety of print orientations. Print designations were assigned to the test specimen based on the corresponding orientation.

Figure 1 shows the print orientation and the naming convention that was used for the tests. The squares in Figure 1 show the stage upon which the model is built and the coordinate system of the printer is displayed accordingly. "flat" parts were printed flush with the board, "vert" parts were printed perpendicular to the board, and "Z" parts were printed full length vertically. The print head is free to move in the X-Y plane, which allows for controlled deposition of the material, but is fixed in the *Z*-direction so the stage steps down to allow for the material to be stacked vertically.

Typically, fatigue tests are conducted with a rapid cyclical loading so that a high number of cycles can be accomplished in a relatively short time. However, to achieve the detailed understanding of the mechanical load on the material, a tensile tester (Tinius Olsen H50KS) was used to provide full stress-displacement history of each load cycle. According to the UNI EN ISO 527-1 (1997) standard, tests are to be conducted at a strain rate of 1 mm/min (approximately 0.039 in/min) to ensure strain rate values below $2.7 \times 10^{-3} s^{-1}$ which is representative of the worst working conditions for polymers (Berti and D'Angelo, 2010). However, at this rate each specimen would take an exorbitant amount of time to complete such a high number of cycles, so the setup was modified so that each specimen was pulled at a rate of 25.4 mm/min (1 in/min) and then relaxed at 12.7 mm/min (0.5 in/min). Figure 2 shows a typical tension-relaxation cycle, while also displaying the displacement rate. The actual time necessary for each cycle varied with the maximum force being tested from specimen to specimen, but the time for one cycle was on the same order. For each test, data were recorded for force (pounds), displacement (in), and time (s).

The H50KS was controlled using its control and data acquisition software, Test Navigator, and a test program was written to cycle the tensile force loading between zero and a predefined percentage of the test sample's ultimate stress. Thus, the sample is nominally under tensile or neutral loads. The controller is designed with a force feedback to keep the test within the desired range. The maximum number of cycles for each test run is set to 10,000 to prevent data overflow or corruption in the Test Navigator software. For longer run cycles, data-subsets of 10,000 cycles are then appended to form the complete dataset. A Tinius Olsen load cell with a maximum force of 50 kN was used. Tinius Olsen HW21 wedge style cross-hatched grips were used for securing the specimen (Figure 3).

Each orientation had four specimens that were tested in the tensile tester. The first specimen of each set was pulled until fracture to determine the ultimate stress of each direction. The remaining three specimens were cycled at 80, 60, and 40 percent nominally of their respective ultimate stresses. It should be noted that the force-feedback control is not perfect, resulting consistent overshoot of the target force from the desired set-point values. As stated in the introduction, due to the time-consuming nature of cyclical load experiments using a tensile tester, only one specimen is used for each print orientation and maximum load percentage. This is deemed reasonable since the objective of this research is to investigate the trends, if any, of the fatigue properties of the FDM ABS materials rather than characterization of a specific material property. Figure 4 shows the detail of how the test specimens were clamped for the tensile tests conducted in addition to its dimensional scale.

Theory

The engineering stress assumption of constant cross-sectional area (initial gauge cross-section) is used for all the data reported here. This approximation is used due to the difficulty in measuring the area changes in real-time. Similarly, the strain

Figure 1 Notation of the nine print orientations used for testing and the square outline representing the stage XY plane

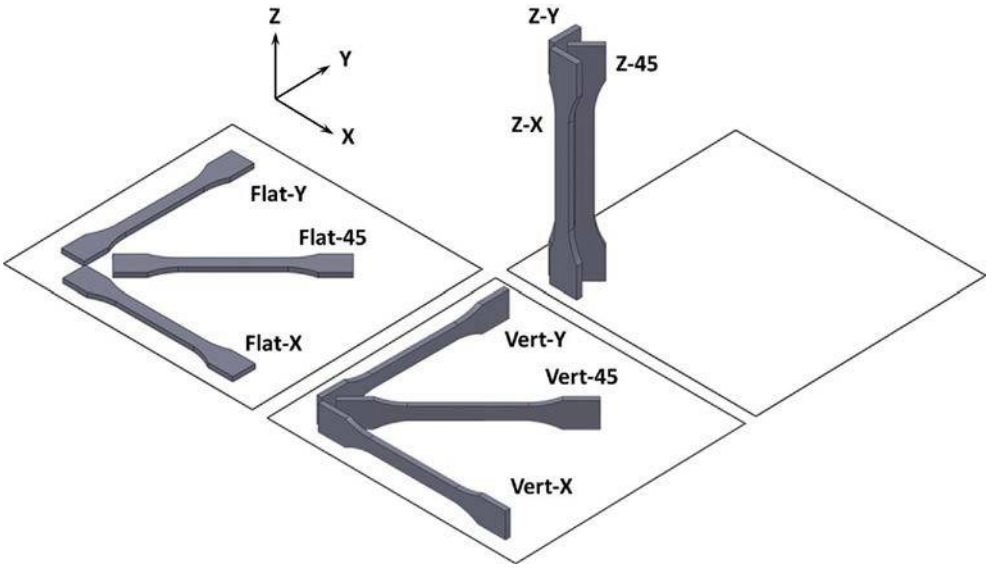

Figure 2 Time history of a typical pull cycle

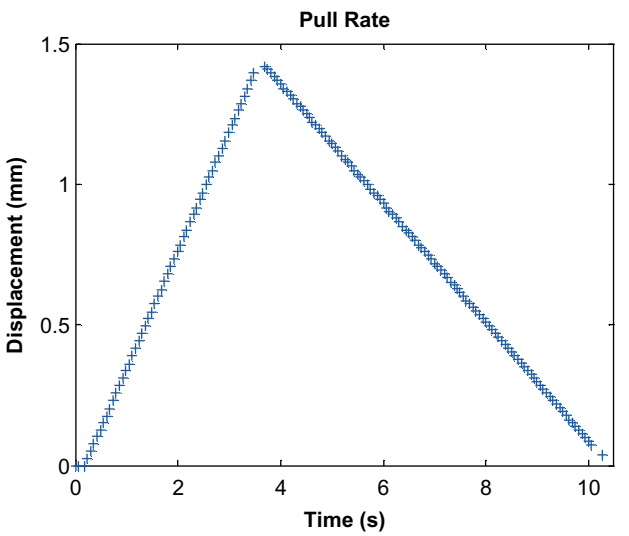

Note: ABSplus Flat-X 60 percent of ultimate

Figure 3 The Tinius-Olsen H50KS tensile testor used for load cycling of the FDM specimen

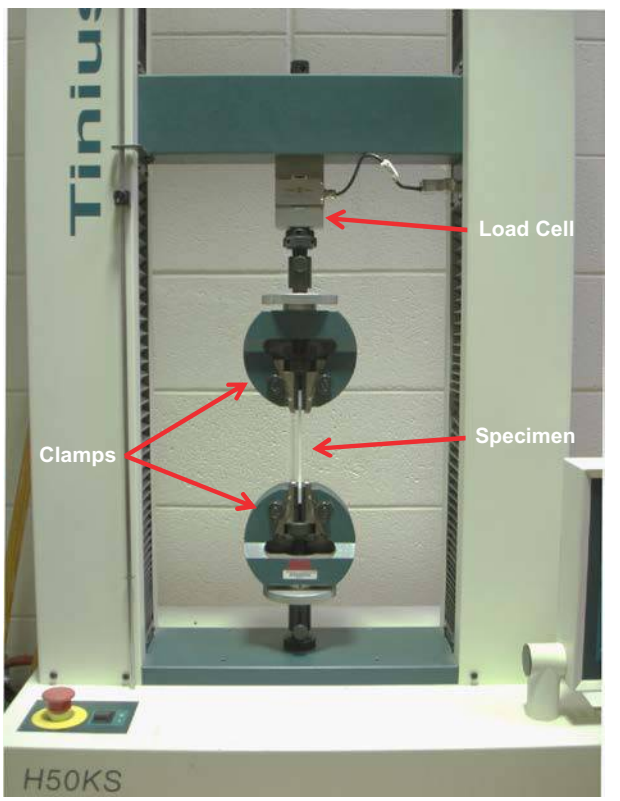

Note: The 50 kN loadcell and the top clamp is mounted on a verticle traverse while the bottom clamp is fixed to the machine frame

recorded should technically be based on the gauge section of the dog bone sample. However, the strain data used is based on the total displacement of the vertical traverse with the clamped specimen and normalized by the gauge length. Thus, the reported values of stress have a tendency of being undervalued and strain being overvalued. Nevertheless, the key goal of the research reported here is to identify the characteristics of the stress-strain properties of the FDM material, which does not depend on the exactness of these values based on ideal definitions.

The area under the stress strain curve during loading is the strain energy per unit volume imparted into the material. Conversely, the area under the unloading curve is the energy released by the material. These two stress-strain curves, and thus their respective areas, are equal for a perfectly elastic material. However, for non-perfectly elastic materials, the interpretation of the stress-strain curves and their respective strain energies are much more varied and complex. For example, for a material strained under its plastic region, the energy imparted into the material will exceed the energy released due to irreversible mechanisms, thus resulting in dissipated heat (Roylance, 2001). Furthermore, both strain

Figure 4 The flat dog-bone specimen based on the UNI EN ISO, 527-1-1997 standards and its reference dimensions

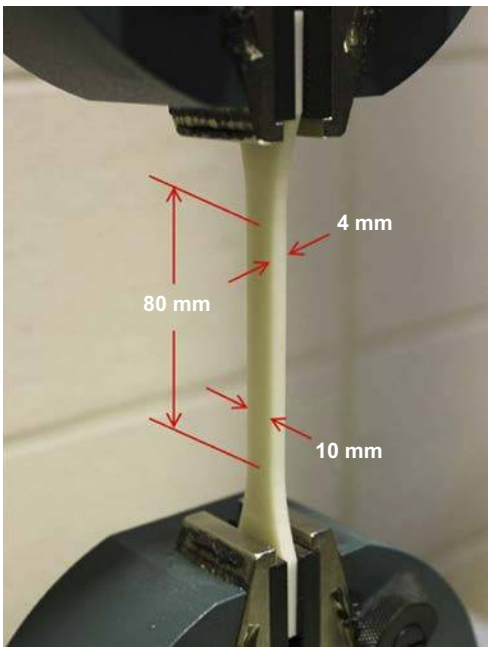

hardening and softening may be present, complicating the analysis of the material behaviors by their strain energies.

The total area under the stress-strain curve up to fracture is termed the modulus of toughness which is the energy needed to completely fracture the material (Roylance, 2001). When the strain exceeds the yield point, the material is deformed irreversibly, so that some residual strain will persist even after unloading. Thermoplastic materials exhibit various forms of plastic behavior. Polymer chains stretch, rotate, slide, and disentangle under load which results in the drop in stress shown in all four trends in Figure 5. When thermoplastics are stressed, it can often result in a light colored (white or grayish) translucent or opaque region which is due to a phenomenon

Figure 5 Stress-strain curve of various materials mention in the writing that the modulus of toughness can vary from pull to pull due to variation of the ultimate strain

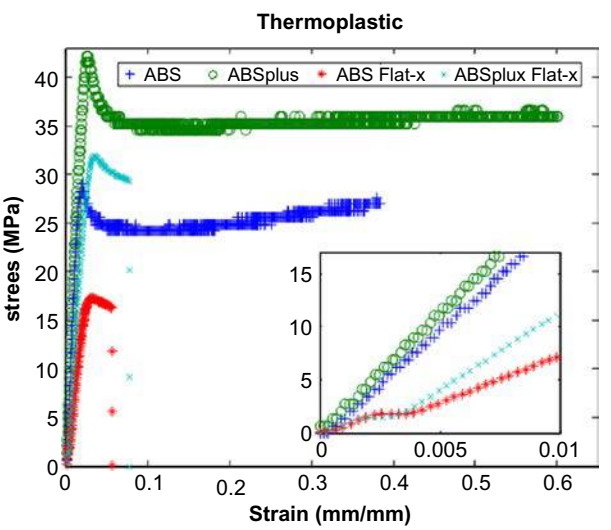

called crazing. Crazing occurs in thermoplastics when localized regions of plastic deformation occur in a direction perpendicular to that of the applied stress which leads to the formation of microvoids (Askeland, 2011). Crazes are different than cracks in that they can still support an applied stress. In the case of elastomers, the stress-strain curve is unique because of the chain uncoiling of the cross-linked polymer. While the trends for *ABS* Flat-X and *ABSplus* Flat-X in Figure 5 (inset) are very similar to that of an elastomer, it is likely not the reason for the relationship based on the recorded data and will be discussed in the analysis section.

Cyclic uniaxial tension and retraction tests of polymers have been conducted and that failure is a result of multiple other aspects, including viscous shear and microvoids (Bartzcak, 2005; Hiss *et al.*, 1999; Hizoum *et al.*, 2011). Data collected for this experiment supports the distinction between bulk polymer characteristics vs those due to FDM layering and the associated directionally dependent properties. Figure 5 shows the stress-strain plots for bulk ABS and ABSplus filaments used by the FDM (1.753 mm diameter and 149.225-mm gauge length) as well as two single-pull dogbones (ABS/ABSplus Flat-X) for comparative purposes in the discussion section. Notice that the filaments exhibit the classical stress-strain behavior of amorphous polymers below its glass transition temperature (Askeland, 2011), where the initial plastic region is followed by strain softening (drop from peak) and then the subsequent straining hardening (slow rise) until fracture.

The difference in material properties between the filament and the printed material is due in large part to the welding kinetics of the 3D printer. One of the more noticeable flaws was sub-perimeter defects which are voids left around the edges when the raster segments turn around during printing. Methods for minimizing these voids are "ploughing" into the perimeter resulting in overlap or modifying the toolpath geometry to force more material into the corners and fill gaps (Agarwala *et al.*, 1996). Another defect can occur when the fill pattern is not completely solid because the spacing and tolerances do not add up to 100 percent which results in an air gap incomplete bonding between two layers. Flaws of this nature would not likely occur for printed dogbones because the termination of the raster segment is in the clamped portion of the specimen and failure rarely occurs in this region. Vector length and time between layers can also play an important role since there is significant temperature decay in the previously printed material temperature which may result in insufficient bonding between adjacent lines resulting in weak interfaces (Agarwala *et al.*, 1996). Also, it was assumed that the flow rate, temperature and filament diameter were optimal during the printing process as variation in each one of these aspects can result in inferior properties. All of these defects are a result of the raster pattern and could be controlled by modifying the prescribed fill pattern. However, the raster patterns were not edited, leaving the printed dogbones in their unaltered state, standard defects included. These defects can, and likely do, act as stress concentrations which result in failure of the printed material at a lower stress than the raw filament material.

Fatigue data

All samples were tested in uniaxial tension and retraction between controlled minimum and maximum force levels. Where it was possible, the ultimate stress was tested multiple times, by a single pull until rupture, for each specimen

to determine the repeatability of the tensile test. For the orientations with repeated tests, the ultimate stress was within ±3 percent, indicating that the tests were repeatable. Due to their high-aspect ratio and print orientation, parts fabricated in the "Z" direction were problematic in both the ABS and ABSplus materials. The older dimension printer was not able to successfully print the dogbones because of the high-aspect ratio. As the print achieved near 50 percent completion the part would start to bow or even topple over, resulting in a partially completed part with the remaining ABS spooling out into the chamber. This resulted in an insufficient sample size for data collection. The Dimension Elite, however, was able to completely print the dogbone specimens in this orientation with only minor trouble, where occasionally a few of the parts toppled over during printing. However, inconsistent results were measured since it depends predominantly on the bonds between the layers rather than the material itself, further confirming that the material strength of the material is much higher and more consistent than the fused bonding between successive layers. Shown in Figure 6 is a typical pull history for an *ABS* dogbone (Flat-X at 80 percent of ultimate stress) while the material is cyclically loaded until failure. Similarly, Figure 7 shows the corresponding *ABSplus* dogbone pull history for the same orientation and percentage of maximum ultimate stress. Note that the actual maximum stresses set for the two materials of the same print orientation are not identical due to their differences in the ultimate stresses; in this case they are 1.4×10^6 Pa and 2.75×10^7 Pa for *ABS* and *ABSplus*, respectively. Table I also shows the corresponding ultimate stresses measured from the 100 percent case(s), where those with multiple samples are averaged.

Analysis

A homogeneous test specimen will fail directly in the middle where the stress is highest. However, Figure 8 shows that the point of failure varied along the length of the dogbone neck. RP of these specimens resulted in flaws which acted as stress concentrations and severely impacted the material properties. The failure profile was influenced by the print orientation which dictated the raster fill pattern. Dogbones printed in the "flat" direction had a jagged failure profile across the neck because of the cross-hatched pattern which delaminated as the dogbone was stressed. "vert" test specimens had a fairly straight failure profile because there was no cross-hatching across the neck. The printed material is opaque where it has been stressed and forms a repeated pattern based on how the dogbone failed.

Figure 6 ABS Flat-X specimen showing the pull history at 80 percent of the ultimate load

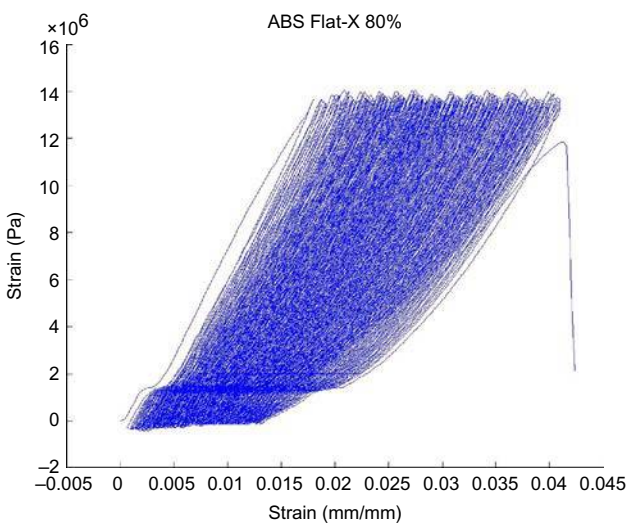

Figure 7 ABSplus Flat-X specimen showing the pull history at 80 percent of the ultimate load

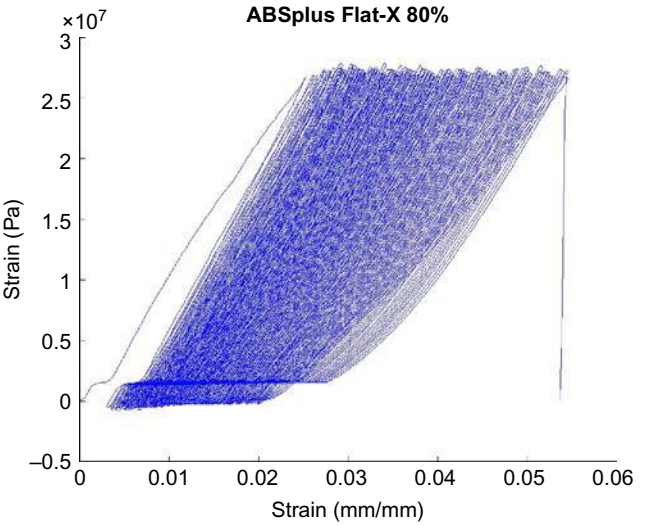

The tensile tester output file, consisting of three columns representing pull force, displacement, and time, respectively, was post-processed using a Matlab script. It converted the force data into stress values by dividing by the gauge area dimensions, converted the pull displacement into strain by dividing by the gauge length, and integrated the area under the pull cycle curves to represent the strain energy. Each pull cycle was indexed and separated into individual up and down strokes, identified by the change in direction of the recorded strain values. The integrationwas performed in piecewise, allowing each up and down stroke strain energy values (Pascals) to be identified. The "quadl" Matlab intrinsic subroutine was used for the integration, which was based on the recursive adaptive Lobatto quadrature with a default tolerance of 1×10^{-6}. The "quadl" subroutine required an interpolation fit ("interp1") of the discrete data from the experiments, which in this case the cubic spline fit was used for each pull stroke.

The stress vs load-cycle-to-break data (Wohler curves) is shown in Figure 9 for the six different orientations of *ABS*. Every data point represents a single specimen that was tested at the given conditions. Complementing the ABS data are those for the *ABSplus*, as shown in Figure 10, collected for the nine print orientations. When comparing Figures 9-10, it is clear that the *ABSplus* material has an overall higher ultimate strength. The *ABS* specimens were between 19 and 25 MPa while the *ABSplus* specimens were around 35-37 MPa. Also, rapid prototyped *ABSplus* dogbones were more isotropic in behavior when compared to ABS dogbones, as evidenced by Figure 9 showing a scatter of data while Figure 10 shows a more tightly grouped set of data. Also noticeable from Figure 9 is that although the vertically printed (Z) directions yield a significant reduction in strength, its trends in the S-N curve parallels the other printed directions. This is surprising since it suggests that

Table I Data collection matrix outlining the ultimate stress (σ_u) and the number of samples tested for each print orientation

	ABS					ABSplus				
	σ_u (Mpa)	100%	80%	60%	40%	σ_u (Mpa)	100%	80%	60%	40%
Flat-X	17.24	1	3	1	1	32.41	2	1	1	1
Flat-Y	18.27	1	1	1	–	32.51	2	1	1	1
Flat-45	19.61	1	1	1	–	33.44	3	1	1	1
Vert-X	23.02	2	1	1	1	34.89	2	1	1	1
Vert-Y	23.43	2	1	1	1	32.51	2	1	1	1
Vert-45	21.26	2	1	1	1	34.58	2	1	1	1
Z-X	–	–	–	–	–	12.90	2	1	1	1
Z-Y	–	–	–	–	–	–	2	–	–	1
Z-45	–	–	–	–	–	–	2	–	–	1

Figure 8 FDM test specimen failure

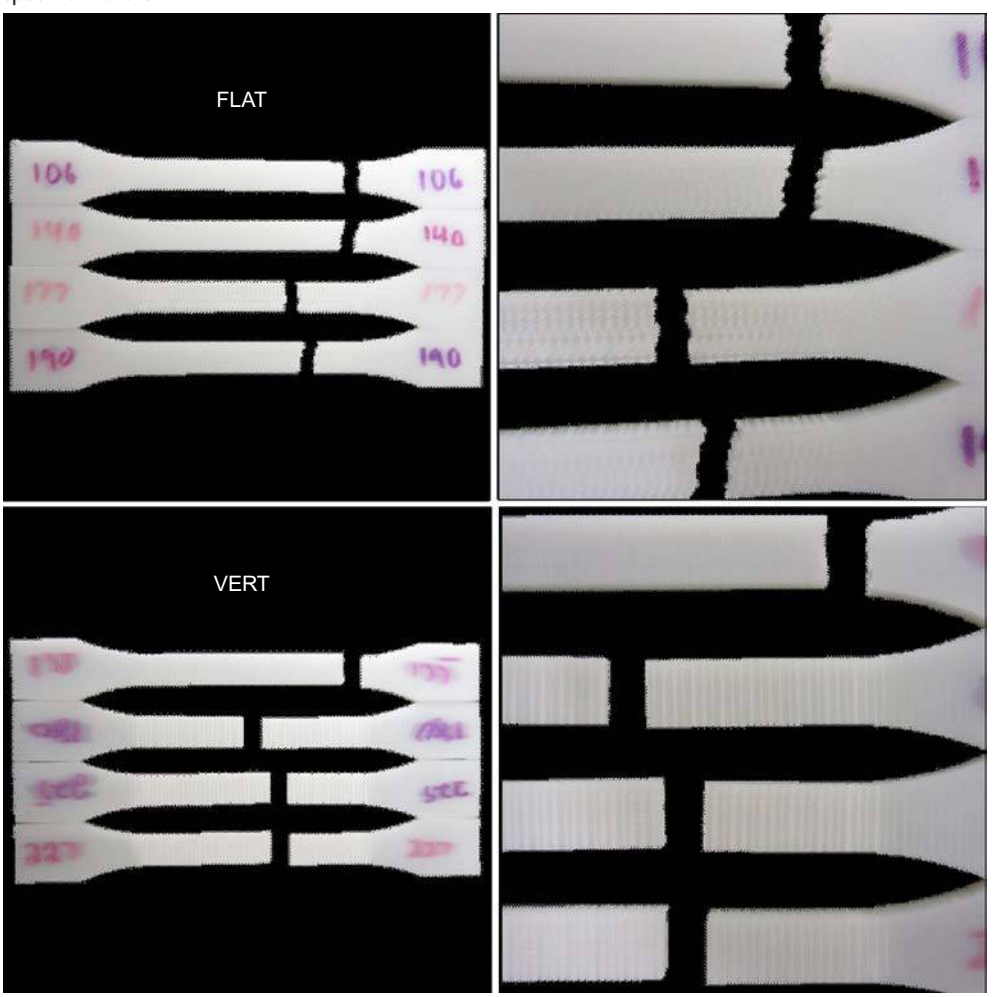

the FDM *ABSplus* parts exhibit parallel fatigue degradation characteristics in all printed principal axes, pointing to a common degradation mechanism regardless of print direction. Another worthwhile observation is that at approximately 40 percent of the ultimate stress the number of cycles until failure is roughly in the order of one thousand.

Two distinctly different trends were observed for the compiled modulus of toughness vs cycles plots, exemplified here using the trends for nominal cyclical tensile loading of 251 pounds and 188 pounds for *ABSplus* Flat-X; 80 and 60 percent of the ultimate load, respectively. The " + " represents the area under the loading curve, while the "o" represents the area under the unloading curve when the specimen is being relaxed back to zero force. The directionality of the unloading curve yields a negative strain energy, which is reported here as positive values to better compare the two opposing strokes. The first trend, shown in Figure 11(a) was a grouping of the data which formed horizontal bands where the area under the positive curve, " + ", was always less than the area under the corresponding negative curve, "o", up to the specimen fracture.

Figure 9 ABS S-N curves for six different orientations

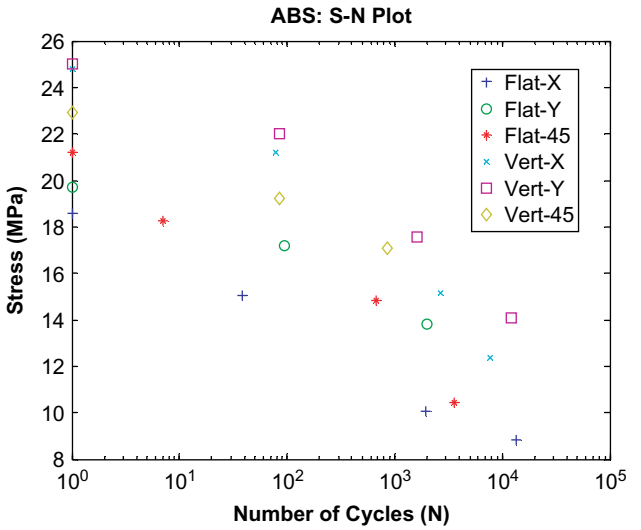

Figure 10 ABSplus S-N curves for seven different orientations

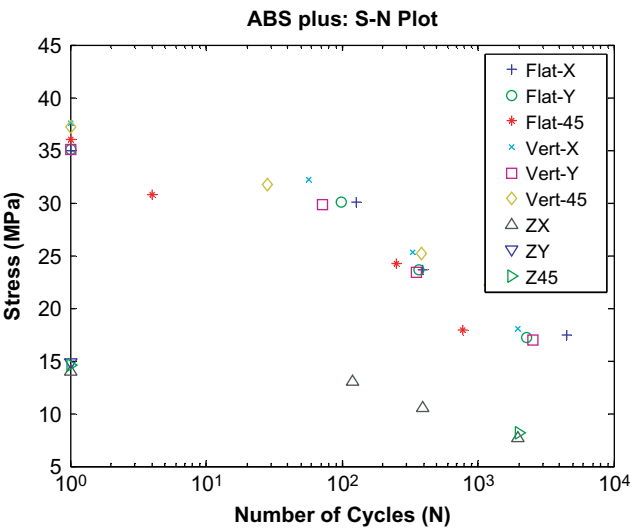

The second trend, shown in Figure 11(b), occurred when the cyclical stress was closer to the ultimate stress with its corresponding low number of cycles before fracture. As the specimen was stretched, the areas under the up and down portions of the stress-strain curve began to deviate from each other. The upstroke yielded larger positive strain energy than the relaxing stroke until the failure of the specimen. One of these two trends was consistently present for all the print directions tested.

The positive and negative strain energies were summed for each cycle to determine the total strain energies of each trial. Figure 12 is a plot of the total strain energy against the cyclical loading that was used to conduct the tests. Every orientation had an inherent trend that started out negative at lower percentages of the ultimate stress but crossed into the positive when cycled between 60 and 80 percent, with the cross-over interpolated to be around 70 percent for almost all directions and both ABS types. Thus, it was expected that the trends described in the previous paragraph and supported by Figure 11 related to this cross-over at 70 percent. The magnitude of the total strain energy for *ABS* was noticeably higher than that of *ABSplus*, which was consistent with the Wohler curves which showed the ABS specimens lasted more load cycles before break. Another interesting note was the absolute value of the *ABSplus* total strain energy for Flat-X was always the highest while Flat-45 was the lowest, before and after the cross-over. Notice though that the strain energy accumulated for all the single-pulled dogbones printed in any of the tested directions were significantly less than the inherent material itself, as can be seen in Figure 12. This suggests that there is a tremendous amount room for improvements when it comes to using FDM ABS parts to absorb loads. Furthermore, cyclical loads experiencing loads of lower percentage of ultimate stress (such as less than 80 percent) exhibited a total strain energy of negative magnitude, indicating a totally different failure mechanism. Closing the gap in total strain energy of the printed material vs the native material may be the follow-on motivation in improving FDM parts designed specifically to perform under cyclical loads. However, an adequate model to explain the negative total strain energies (as opposed to the positive values

Figure 11 ABSplus Flat-X showing the strain energy plots at approximately

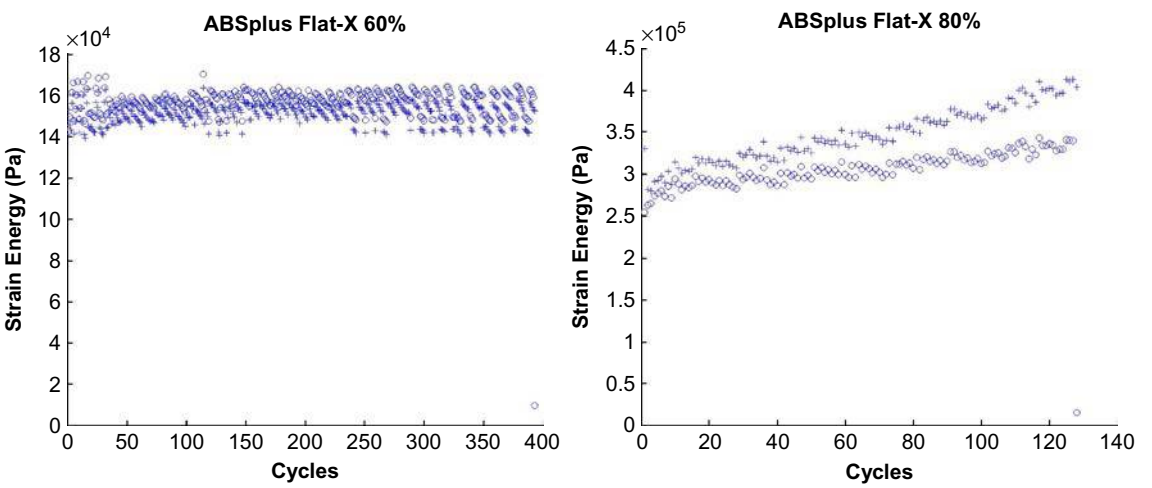

Notes: (a) 60 percent; (b) 80 percent of the ultimate load

Figure 12 Strain energy vs percent of ultimate load

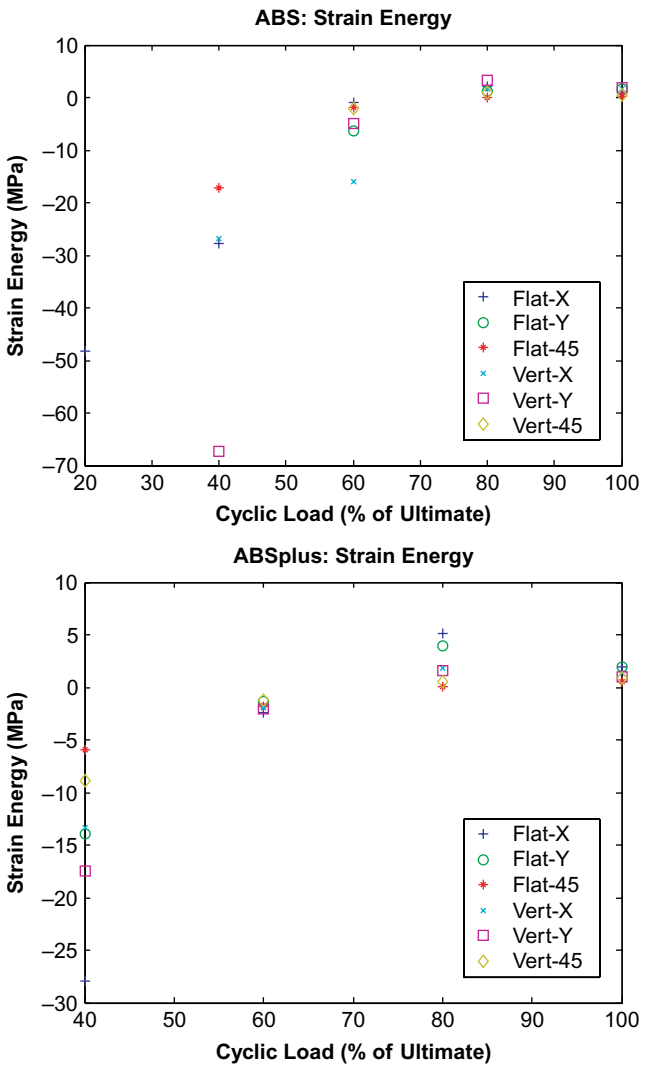

from single pulls) of cyclical loads at low percentages of its ultimate stress must also be addressed.

Lastly, going back to the stress-strain curves, it appeared that the dogbones experienced chain uncoiling, common in elastomers and some thermoplastics, at about 0.0025-0.005 strain, as can be seen in Figure 5. However, in the same figure, the inherent ABS/ABSplus material pulled (of filament cross-section) did not show any chain uncoiling, indicating that some other mechanism was the cause of this phenomenon. Since his trend of exhibiting constant stress while under strain was visible in every different orientation tested, it suggests that it was a result of the print orientation, path, and layering.

Conclusion

The ultimate stress for the *ABS* printed specimens ranged from 50 to 80 percent of the ABS wire data. *ABSplus* printed specimens were much better in that they ranged from 75 to 80 percent (omitting the *Z*-direction), and overall higher and narrower range, of the ABSplus wire data. While tensile stress remained relatively similar to the respective material value, strain energy was far less. For *ABS* printed parts strain energy ranged from 3.4 to 19.7 percent of the ABS material and *ABSplus* printed parts strain energy ranged from 1.8 to 7.4 percent of the ABSplus material. From these two trends it was obvious that the printed parts lose quite a bit of ductility during fabrication which leaves room for potential improvement of the material properties. A particularly interesting trend was the total energy vs nominal percent of ultimate stress. All of the tests followed a parabolic trend that seemed to peak at around 80 percent of the ultimate load. The strain energy was obviously positive at 100 percent of the ultimate load, but around 70-75 percent the strain energy began trending into the negative region. It should also be noted that while printed *ABSplus* material had a higher tensile stress, it may exhibit lower strain energies (cyclical or single pulls) depending on print directions, which can be observed in Figures 12 and 13.

Further work

In the work presented here, the strain rates used for the cyclical load experiments were based on practicality rather than on theoretical or empirical basis. One follow-on approach is to focus on a single type of specimen (such as *ABSplus* Flat-X) under a range of strain rates to isolate the effect, if any, from dynamic loads. One possibility is that the total strain energy may be dependent on the strain rate. It is also interesting to study whether the cross-over in the reported total strain energies (Figure 11) at 70 percent is truly independent of other load parameters, inclusive of the change in the strain rate. Expanding on it, is this phenomenon unique due to the layering process of the RP ABS materials, or is a universal characteristic of other materials? Current research by the author is focused on exploring the latter question on common metallic materials and bulk plastics. Furthermore, if the effect of increasing strain rate is less consequential to the measure fatigue characteristics then it allows for the possibility of a statistical approach of testing multiple samples to build confidence in the data. Another interesting focus would be on relating the effect of the FDM process on its fatigue characteristics, such as quality of the weld, printing environment, and printed geometries and voids. Without doubt there is a lot of room for future development in understanding the fatigue characteristics and mechanics of RP material and parts.

Figure 13 Comparison of strain energies between printed and wire specimens for both ABS and ABSplus materials

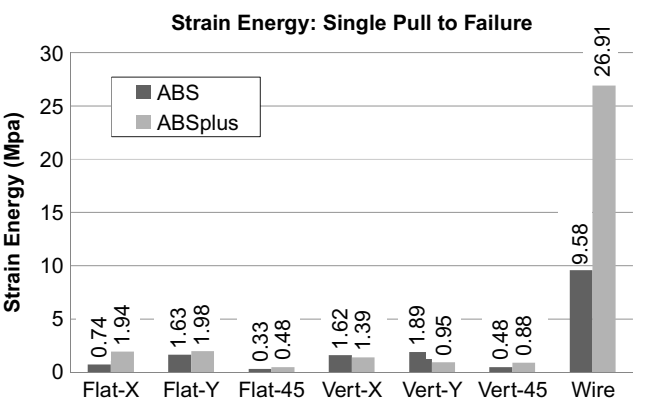

References

Agarwala, M., Vikram, J. and Noshir, L. (1996), "Structural quality of parts processed by fused deposition", *Rapid Prototyping Journal*, Vol. 2 No. 4, pp. 4-19.

Ahn, S.H. and Montero, M. (2002), "Anisotropic material properties of fused deposition modeling ABS", *Rapid Prototyping Journal*, Vol. 8 No. 4, pp. 248-257.

Berti, G. and D'Angelo, L. (2010), "Mechanical characterization of PA-AL_2O_3 composites obtained by selective laser sintering", *Rapid Prototyping Journal*, Vol. 16 No. 2, pp. 124-129.

Ciocca, L. and Fantini, M. (2009), "Immediate facial rehabilitation in cancer patients using CAD – CAM and rapid prototyping technology: a pilot study", *Support Care Cancer*, Vol. 18, pp. 723-728.

Crump, S.S. (1992), *Aparatus and Method for Creating Three-Dimensional Objects*, Patent 5,121,329, Stratasys, Eden Prairie, MN.

Danehy, P.M. and Alderfer, P.W. (2008), "Fluorescence imaging and streakline visualization of hypersonic flow over rapid prototype wind-tunnel models", *Journal of Aerospace Engineering*, Vol. 222 No. 5, pp. 637-651.

Fortus (2007), *ABS*, Stratasys, Eden Prairie, MN.

Fortus (2011), *ABSplus*, Stratasys, Eden Prairie, MN.

Hiss, R., Hobeika, S., Lynn, C. and Strobl, G. (1999), "Network stretching, slip processes, and fragmentation of crystallites during uniaxial drawing of polyethylene and related copolymers: a comparative study", *Macromolecules*, Vol. 32 No. 13, pp. 4390-4403.

Hizoum, K., Rémond, Y. and Patlazhan, S. (2011), "Coupling of nanocavitation with cyclic deformation behavior of high-density polyethylene below the yield point", *Journal of Engineering Materials and Technology*, Vol. 133.

Hull, C.W. (1986), *Apparatus for Production of Three-dimensional Objects by Stereolithography*, Patent 4,575,330, UVP, Inc., San Gabriel, CA.

Kroll, E. and Dror, A. (2011), "Enhancing aerospace engineering students learning with 3D printing wind tunnel models", *Rapid Prototyping Journal*, Vol. 17 No. 5.

Owida, A. and Chen, R. (2011), "Artery vessel fabrication using the combined fused deposition modeling and electrospinning techniques", *Rapid Prototyping Journal*, Vol. 17 No. 1, pp. 37-44.

Roylance, D. (2001), *Stress-Strain Curves*, Massachusetts Institute of Technology, Cambridge, MA, 02139. 23 August.

Further reading

Bartczak, Z. (2005), "Effect of chain entanglements on plastic deformation behavior of linear polyethylene", *Macromolecules*, Vol. 38 No. 18, pp. 7702-7713.

Tinius, O. (2010a), *Benchtop Materials Testing Machines*, Bulletin 140-D, Horsham, PA.

Tinius, O. (2010b), *Wedge Style Tensile Grips*, Bulletin TD-1001, Horsham, PA.

Corresponding author

John Lee can be contacted at: jbl003@uark.edu

This article has been cited by:

1. Boparai Kamaljit Singh, Kamaljit Singh Boparai, Singh Rupinder, Rupinder Singh, Singh Harwinder, Harwinder Singh. 2016. Development of rapid tooling using fused deposition modeling: a review. *Rapid Prototyping Journal* **22**:2, 281-299. [Abstract] [Full Text] [PDF]
2. Singh Boparai Kamaljit, Kamaljit Singh Boparai, Singh Rupinder, Rupinder Singh, Singh Harwinder, Harwinder Singh. 2016. Experimental investigations for development of Nylon6-Al-Al2O3 alternative FDM filament. *Rapid Prototyping Journal* **22**:2, 217-224. [Abstract] [Full Text] [PDF]
3. M. Faes, E. Ferraris, D. Moens. 2016. Influence of Inter-layer Cooling time on the Quasi-static Properties of ABS Components Produced via Fused Deposition Modelling. *Procedia CIRP* **42**, 748-753. [Crossref]
4. Mst Faujiya Afrose, S. H. Masood, Pio Iovenitti, Mostafa Nikzad, Igor Sbarski. 2015. Effects of part build orientations on fatigue behaviour of FDM-processed PLA material. *Progress in Additive Manufacturing* . [Crossref]
5. Haixi Wu, Yan Wang, Zhonghua Yu. 2015. In situ monitoring of FDM machine condition via acoustic emission. *The International Journal of Advanced Manufacturing Technology* . [Crossref]
6. Wenzheng Wu, Peng Geng, Guiwei Li, Di Zhao, Haibo Zhang, Ji Zhao. 2015. Influence of Layer Thickness and Raster Angle on the Mechanical Properties of 3D-Printed PEEK and a Comparative Mechanical Study between PEEK and ABS. *Materials* **8**:9, 5834-5846. [Crossref]
7. Sophia Ziemian, Maryvivian Okwara, Constance Wilkens Ziemian. 2015. Tensile and fatigue behavior of layered acrylonitrile butadiene styrene. *Rapid Prototyping Journal* **21**:3, 270-278. [Abstract] [Full Text] [PDF]